https://doi.org/10.5194/tc-2020-349
Preprint. Discussion started: 2 December 2020

The Cryosphere Discussions
Open Access
EGU

Simulating the internal structure of the Antarctic Ice Sheet - towards a spatio-temporal calibration for ice-sheet modelling.

Johannes Sutter[1], Hubertus Fischer[1], and Olaf Eisen[2,3]

[1]Climate and Environmental Physics, Physics Institute, and Oeschger Centre for Climate Change Research, University of Bern, Bern, Switzerland
[2]Alfred Wegener Institute Helmholtz-Centre for Polar and Marine Research, Bremerhaven, Germany
[3]Department of Geosciences, University of Bremen, Bremen, Germany.

Correspondence: Johannes Sutter (johannes.sutter@climate.unibe.ch)

Abstract. Ice Sheet Models are a powerful tool to project the evolution of the Greenland and Antarctic Ice Sheets, and thus their future contribution to global sea-level changes. Probing the fitness of ice-sheet models to reproduce ongoing and past changes of the Greenland and Antarctic ice cover is a fundamental part of every modelling effort. However, benchmarking ice-sheet model data against real-world observations is a non-trivial process, as observational data comes with spatio-temporal gaps in coverage. Here, we present a new approach to assess the ability of ice-sheet models which makes use of the internal layering of the Antarctic Ice Sheet. We simulate observed isochrone elevations within the Antarctic Ice Sheet via passive Lagrangian tracers, highlighting that a good fit of the model to two dimensional datasets does not guarantee a good match against the three dimensional architecture of the ice-sheet and thus correct evolution over time. We show, that paleoclimate forcing schemes commonly used to drive ice-sheet models work well in the interior of the Antarctic Ice Sheet and especially along ice divides, but fail towards the ice-sheet margin. The comparison to isochronal horizons attempted here reveals, that simple heuristics of basal drag can lead to an overestimation of the vertical interior ice sheet flow especially over subglacial basins. Our model-observation intercomparison approach opens a new avenue to the improvement and tuning of current ice-sheet models via a more rigid constraint on model parameterisations and climate forcing which will benefit model-based estimates of future and past ice-sheet changes.

1 Introduction

A core motivation of the ice-sheet modelling community is to provide meaningful projections of future sea level rise. Towards this goal, great strides have been made in improving ice-sheet models (ISMs) to capture current and past modes of ice-sheet dynamics (Pattyn, 2018). However, at this point projections of the future behaviour of the Greenland and Antarctic Ice Sheet under global warming are divergent depending on model physics, initialisation and the choice of climate forcing (Seroussi et al., 2019, 2020; Goelzer et al., 2020). This has important ramifications for model-based estimates of future sea level change especially in the case of the Antarctic Ice Sheet due to its potentially highly nonlinear response to climate warming (Garbe et al., 2020). Despite major improvements, ISM simulations today are constrained by incomplete boundary conditions such as uncertainties in the bedrock relief and geothermal heat flux, fragmental information on past and present climate conditions (es-

https://doi.org/10.5194/tc-2020-349
Preprint. Discussion started: 2 December 2020

pecially with regard to ocean circulation underneath ice shelves) and model heuristics such as parameterisations of grounding line dynamics, ice flow and ice-shelf calving processes. To overcome these limitations, ISMs are usually tuned to observations of the past and present state of an ice-sheet. Well established two dimensional data benchmarks used in ice-sheet modelling are e.g. the BEDMAP2 (Fretwell et al., 2013), BedMachine (Morlighem et al., 2017, 2020) and MEaSUREs (Joughin et al., 2015, updated 2018; Mouginot et al., 2017, updated 2017) data sets for Antarctica and Greenland, which provide a continental coverage of ice-sheet geometry and surface flow. Ideally, ISMs are not only tuned to the present state of an ice-sheet but also to paleo-horizons to ensure their capability to capture an ice-sheet's evolution under climate conditions differing from the Common Era (e.g. DeConto and Pollard (2016); Sutter et al. (2019); Seroussi et al. (2019); Edwards et al. (2019)). Typical target climate epochs are the Last Glacial Maximum (LGM) with relatively well constrained grounding-line margins in Antarctica (Bentley et al., 2014) and paleo ice sheet elevation proxies which can be utilised as a tuning target (Albrecht et al., 2020). Furthermore, sea level reconstructions from the Last Interglacial (LIG) can give an indication of ice loss in Antarctica and Greenland (Dutton et al., 2015). Such benchmarks are necessary to not only get the currently observed geometry and velocity right, but also initialise the ice sheet's full state as good as possible by taking into account its paleo-evolution.

Using the above mentioned tuning targets allows to simulate an ice-sheet in line with the present day observed surface properties and proxy data from the past millennia. However, the notion that a good fit to spatial datasets of the Common Era and proxy targets in the past guarantees the model's ability to respond accurately to future climate changes is debatable. Due to the complexity of ice-sheet-climate interactions, lack of spatial data sets for past climate states and uncertainties in paleo-proxy based ice-sheet and sea level reconstructions, it is still challenging to create a proper initial ice-sheet configuration from which its future evolution can be adequately simulated (Seroussi et al., 2019, 2020). For example, tuning the ice-sheet to the observed present state (e.g. via inversion for basal drag) to match the current ice-sheet topography and surface flow does not guarantee the accurate reproduction of e.g. internal flow, ice temperature distribution and basal friction. It also could lead to overfitting of parameters relevant to ice flow in scope of uncertain boundary conditions such as geothermal heat flux, sub-shelf ocean temperatures, and surface mass balance. Without inversion the modelled present day topography can differ from the observed state by several hundred meters of ice thickness on which basis it is difficult to interpret model-based sea level projections. Fundamentally, every ISM application is an ill-posed problem with non-unique solutions. Therefore, overfitting to a set of observables could lead to an initial ice-sheet configuration dominating the projected response to the applied climate forcing (Seroussi et al., 2019), especially over decadal to centennial timescales. Discrepancies in the initial state with respect to the actual real world ice-sheet can propagate and multiply during the model simulation due to the intrinsic nonlinearities of the system. Even a near-perfect match to present day 2D or 1D observable state variables can conceal overtuning of the model due to weakly constrained boundary conditions, e.g. uncertainties in the climate forcing or geothermal heat flux (Burton-Johnson et al., 2020; Talalay et al., 2020). To reduce the effect of these limitations, we propose an additional data benchmark for ISMs which provides spatio-temporal constraints incorporating the paleo-evolution of an ice-sheet and complements the hitherto used 2D and 1D tuning targets.

Paleo-surfaces within ice sheets are created by simultaneous deposition of impurities at the ice-sheet's surface. These are widely observable by radio-echo sounding. The internal horizons (isochrones) of ice-sheets provide a spatio-temporal calibra-

https://doi.org/10.5194/tc-2020-349
Preprint. Discussion started: 2 December 2020

tion for ISMs, as they are formed by the three dimensional flow patterns of the ice-sheet over time and therefore integrate all aspects of an ice-sheet's evolution in one observable. Isochrones are mapped by radar observations as individual radar reflections within the ice and are subsequently dated for example by using tie points to ice core chronologies (crossover points) or distinct reflectors such as dated volcanic eruptions. An ice-sheet wide coverage of such traced and dated englacial layers, as envisioned by the SCAR action group AntArchitecture (Bingham, 2020) would be an invaluable tuning benchmark, which both constrains the climate forcing as well as the simulated ice flow more tightly than hitherto employed 2D or 1D data targets. So far, isochrones have been used in or with ice-flow models (1D, 2D or 3D) to reconstruct paleo accumulation patterns and changes, e.g. in Leysinger-Vieli et al. (2011); Cavitte et al. (2018), or to constrain high resolution alpine glacier models (Konrad et al., 2013; Jouvet et al., 2020). Specialised models have been developed to compute isochrone geometry (Hindmarsh et al., 2009) or tailor-made to accurately simulate the internal layering of ice-sheets (Born, 2017). Lagrangian and semi-lagrangian tracer advection has been employed to shed light on the isotopic composition and stratigraphies of the Greenland and Antarctic Ice Sheets (Clarke et al., 2003, 2005; Lhomme et al., 2005a, b; Huybrechts et al., 2007; Goelles et al., 2014; Born, 2017), to identify potential locations of old ice in Antarctica (Passalacqua et al., 2018) and recently to assess past ice sheet instabilities (Sutter et al., 2020) . Despite these achievements, englacial isochrones have not been getting the required attention in the context of tuning targets for continental ISMs (Born, 2017).

In this work, we discuss the ability and limitations of a 3D continental ISM to capture englacial layers and therefore to exploit existing isochrone elevation datasets to constrain ISM results. We compare model results to dated isochrones spanning a large part of the East Antarctic Ice Sheet and discuss how such a comparison can be utilised to improve ISM simulations. Thus, this work does not aim at reconstructing the internal architecture of the Antarctic Ice Sheet as detailed as possible (as e.g. done in Parrenin et al. (2017)), but rather to exploit isochrones as a constraint on model behaviour to improve the modelling of paleo-ice-sheet evolution. In section 2 we give an overview over the observed traced and dated internal layers from East Antarctic radar transects used in this study and introduce the post-processing routine (Lagrangian tracer advection) and the input data. In section 3 we focus on the ice-core deep drilling site Dome C and provide a detailed analysis of the simulated internal layering in comparison to a set of observed layers from four individual radar transects, discussing paleo-accumulation patterns and the impact of ice dynamics. Finally, we expand this view to the whole East Antarctic Ice Sheet in section 4.

2 Approach to modelling Antarctic isochrones

We use ice-sheet model results (Sutter et al., 2019) attained from simulations with the ISM PISM (the PISM authors, 2015; Bueler and Brown, 2009; Winkelmann et al., 2011b) to compute Antarctic isochrone elevations, where we tune the ice-sheet model to match against observational data from present day (PD), the Last Glacial Maximum (LGM) and the Last Interglacial (LIG). Tuning targets include the surface elevation at East Antarctic ice core locales as well as the grounding line extent at the LGM (Bentley et al., 2014), LIG sea level reconstructions (Dutton et al., 2015) and PD sea level equivalent ice volume and grounding line position (Fretwell et al., 2013). We choose selections of traced and dated englacial layers which have crossovers with the EPICA Dome C (EDC), EPICA Dronning Maud Land (EDML), Dome Fuji and Vostok ice-cores. Unfortunately, the

https://doi.org/10.5194/tc-2020-349
Preprint. Discussion started: 2 December 2020

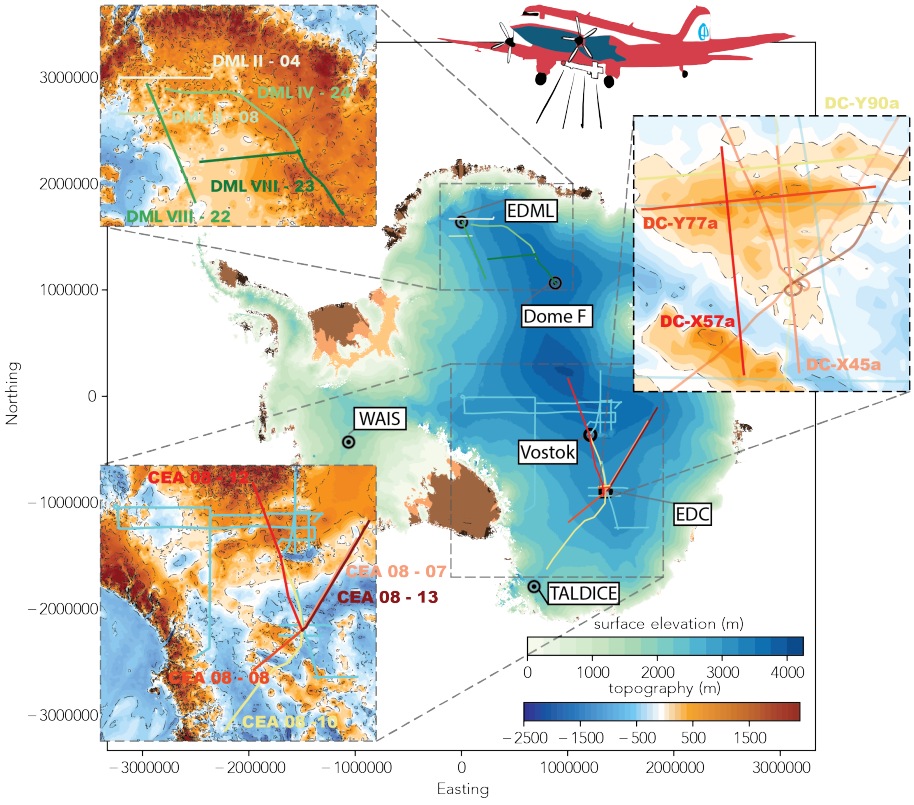

Figure 1. Antarctic topography from BedMachine Antarctica (Morlighem et al., 2020) overlain by radar transects analysed in this study. The enlarged sections highlight three regional clusters which we focus on in the following sections.

number of published and available traced and dated Antarctic isochrones is limited at the current stage, a situation which initiatives like AntArchitecture aspire to improve in the coming years. For this intercomparison we make use of three excellent compilations of dated isochrones (Leysinger-Vieli et al., 2011; Cavitte et al., 2016; Winter et al., 2019) which provide about 95 10,000 km of analysed radar transects covering the past 38 ka to 170 ka BP (see Table 1). With this wealth of information we are able to not only analyse the performance of our model simulations close to ice core locations but also along and across ice divides spanning the whole distance from Dronning Maud Land to the George IV Coast (see Figure 1). The area connected by the radar-transects covers a wide range in the spectrum of bedrock relief, geothermal heat flux as well as climate regimes and ice-sheet elevations. This allows us to analyse the impact of uncertainties in the paleo mass balance, basal melt, 100 ice dynamics and bedrock on modelled isochrone elevations. Table 1 gives an overwiew of the radar-transects used in this work. The Dome C region is included in all three cited studies and provides an excellent region to test the validity of the climate forcing scheme employed by Sutter et al. (2019). The EDC ice core itself provides tight constraints on the age of the isochrones via the AICC2012 chronology (Veres et al., 2013; Bazin et al., 2013) as well as the accumulation history during the last glacial-interglacial cycle (Cavitte et al., 2018). It is important to note that, as the ISM's climate forcing was modulated

https://doi.org/10.5194/tc-2020-349
Preprint. Discussion started: 2 December 2020


The Cryosphere Discussions
Open Access
EGU

Table 1. Overview of analysed isochrones.

Name	Region	Line length (km)	Age (ka)
^{C}DC - X45a,X57a,Y77a,Y90a	Dome C	100	38,48,73,96,130,160
^{W}CEA-7,8,10,12,13	Wilkes Basin - Dome C - Vostok - Dome A	400 - 1800	38, 90, 161
^{W}DML- II-04,II-08,IV-24,VIII-22,VIII-23	Dome Fuji - EDML	200 - 800	38,74
^{LV}DC - 1,2,3	Dome C	50 - 600	36.5,73,130,170
^{LV}V - 1,2,2W,3	Vostok - Dome A - South Pole	50 - 2000	36.5,73,130,170

Isochrones are from Cavitte et al. (2016) (^{C}DC-X45a,X57a,Y77a,Y90a), Winter et al. (2019) (^{W}CEA-7,8,10,12,13,DML- II-04,II-08,IV-24,VIII-22,VIII-23) and Leysinger-Vieli et al. (2011) (^{LV}DC - 1,2,3, ^{LV}V - 1,2,2W,3). The superscripts (^{C,W,LV}) denote the respective publication. The line lengths (x-y) specified in the table vary depending on the transect except for the data from Cavitte et al. (2016) where all transects are 100 km in length. The specified ages are those used in this manuscript but do not represent the complete set of internal layers available in the respective references.

via the EDC deuterium record, we expect the best fit of our computed isochrones to be in the region encompassing this ice core. The areas around EDC, Dome Fuji and EDML are all well sampled by reliable radar observations, therefore providing very accurate estimates of bedrock elevation (Karlsson et al., 2018). This makes it possible to investigate the impact of bedrock uncertainties on the mismatch between observed and computed isochrone elevations. Finally, the transects in the vicinity to faster flowing marine drainage regions (e.g. Wilkes Subglacial Basin) allow for an assessment of model parameterisations of ice flow on the computed isochrone elevation.

2.1 Observation of isochrones

Radar surveys of ice-sheets observe numerous internal layers, i.e., changes in the dielectric properties of the ice, which lead to a partial reflection of the downward propagating radar wave back to the surface. Most of these layers are caused by changes in the conductivity content of the ice by deposition of acids from volcanic eruptions at the surface of the ice-sheet. After volcanic eruptions these depositions usually occur over a few years and are rather homogeneous over spatial scales of 10s to 100s of km. The absence of melting on the Antarctic plateau leads to continuous burrial and, thus, submergence of these conductivity layers, which are typically spread over less than one meter (Eisen et al., 2006). Lateral variations in accumulation rates cause differences in submergence velocities and, thus, to deformation of these initially surface-parallel layers. With increasing depth, the influence of ice dynamics on the (vertical) submergence velocity increases and deforms the layers further.

Radar systems used to map internal layers and the thickness of ice-sheets operate in the range of 10s to 100s of MHz, corresponding to a wavelengths on the order of meters. The width of the observed reflections, caused by the interaction of the electromagnetic radar waves with the conductivity peaks, is determined by the bandwidth or pulse length of the radar systems. They are typically in the range of 0.5 to several tens of meters (Winter et al., 2017).

With increasing depth the internal layers often follow the bed topography in an often smoothed fashion. Thus, the lateral variation of the depth of these internal reflection horizons is usually sufficiently small to be continuously detected with the spatial sampling distance of airborne radar systems. They operate with a horizontal sampling distance in the range of meters

https://doi.org/10.5194/tc-2020-349
Preprint. Discussion started: 2 December 2020

to tens of meters (Winter et al., 2017) and can be traced over hundreds to thousands of kilometres. As each of these layers originates from the same physical change in conductivity, which the ice inherited during deposition as snow at the surface, they are considered isochrones and have the same age along the reflection horizon.

Dating can most reliably be achieved by tying internal layers to ice core sites, where age–depth estimates are available from ice-core proxy analysis. For the comparison of observed and modelled isochrone elevations, the uncertainty of the observed isochrones is an important parameter. Apart from the radar-inherent uncertainties coming along with identifying and continuously tracing the same radar signal for an horizon and the conversion of two-way traveltime to depth, the uncertainty in the ice-core ages and the actual matching procedure between horizons and ice core are the largest sources of error. We use various internal layers in this study. Details on the radar resolution, dating methods and resulting uncertainty can be found in the respective original publications (Cavitte et al., 2016; Winter et al., 2019; Leysinger-Vieli et al., 2011). Based on the analysis performed on five different radar systems by Winter et al. (2017) near EDC, we consider an age uncertainty of around 1 ka (Winter et al., 2019) down to a depth of around 2000 m (roughly 2/3 or the ice thickness), which non-linearly increases with depth towards the bed. This range covers most of the horizons considered in this study. At places where the deepest ice is younger than around Dome C, the age gradient with depth will be less steep towards the bed. Thus, the age uncertainties of the horizons will be lower. We consider this uncertainty always to be smaller than the proposed age derived from the ISM data.

2.2 Large-scale ice-sheet modelling

In order to compute Antarctic isochrones, time resolved 3D velocity data as well as the transient ice-sheet geometry (ice thickness and bedrock topography) are necessary. We therefore ran a paleoclimate model ensemble covering the last 220 ka and make use of previously published model ensemble results covering the last 2 Ma (Sutter et al., 2019). An overview over the experimental setup is provided in Figure 2. The model forcing is described in detail in Sutter et al. (2019) and provides spatio-temporal information on ocean temperatures, surface temperature and precipitation derived from climate snapshots during the LIG (Pfeiffer and Lohmann, 2016) and the LGM as anomaly forcing with respect to the modelled pre-industrial climate state. In between the climate snapshots, surface temperature and ocean temperatures are interpolated on the basis of the EDC deuterium data (Jouzel et al., 2007) (see section 2.3 and Figure 2 in Sutter et al. (2019)). The ISM is run on a 16 km grid with 81 vertical levels except for a present day run which is carried out on an 8 km grid with 101 vertical levels. We employ a combination of the shallow ice (SIA) and shallow shelf (SSA) approximation (SSA+SIA Hybrid; Winkelmann et al. (2011a)) with a sub-grid grounding line parameterisation (Gladstone et al., 2010; Feldmann et al., 2014) to allow for reversible grounding line migration despite using a relatively coarse resolution (Feldmann et al., 2014). For further details regarding the ISM setup see section 2.1 in Sutter et al. (2019). Geothermal heat flux is taken from Shapiro and Ritzwoller (2004) as well as from Purucker (2013); An et al. (2015); Martos et al. (2017). Topography data are from Bedmap2 (Fretwell et al., 2013) except in the present day simulation where we use the new BedMachine-Antarctica dataset from Morlighem et al. (2020). We model isochrone elevations (see 2.3) on the basis of full paleo-ice-sheet model runs (*pal*), the present day snapshot of the latter (*pd-pal*) and a present day equilibrium run (*pd*).

https://doi.org/10.5194/tc-2020-349
Preprint. Discussion started: 2 December 2020

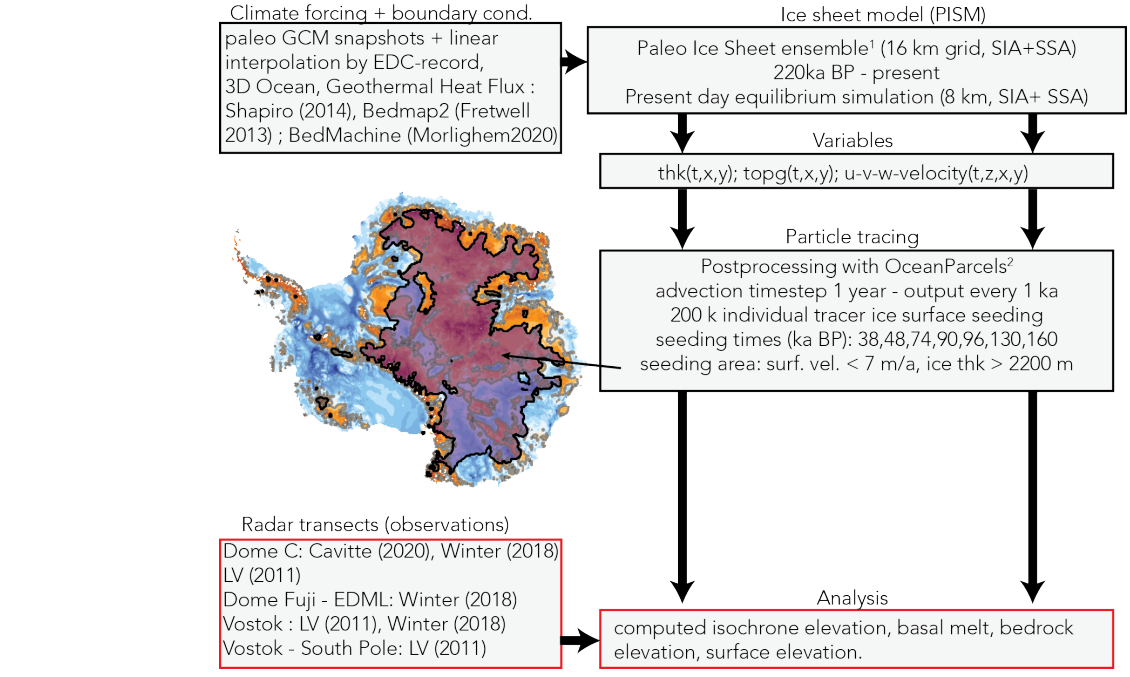

Figure 2. Experimental setup. The left column depicts the input data to the ice-sheet model (climate forcing, geothermal heat flux and initial geometry) and to the data intercomparison (observed radar transects). The contour plot illustrates the area where tracers are seeded (see supplementary video). The right column contains the ice-sheet model specifications, required variables (thickness, bedrock topography and 3D velocity field) for the tracing scheme and the settings used in OceanParcels.

2.3 Lagrangian tracer advection

We employ the open source python software OceanParcels v0.9 (Lange and van Sebille, 2017) which was originally designed to analyse ocean data but can be easily adopted for transient or steady state ISM data. At its core, OceanParcels provides a Lagrangian particle tracking scheme which is computationally efficient and adaptable to a variety of input grids (Delandmeter and van Sebille, 2019). Individual particles tracks are computed following the advection equation (equation 1 in Lange and van Sebille (2017)):

$$\mathbf{X}(t+\Delta t) = \mathbf{X}(t) + \int t + \Delta t_t \mathbf{v}(\mathbf{x},t)dt + \Delta \mathbf{X}_b(t) \tag{1}$$

where $\mathbf{X}$ is position of the particle in space, $\mathbf{v}$ the three-dimensional velocity at the particles' position and $\Delta \mathbf{X}_b(t)$ is the change in position due to "behaviour", which does not play a role in our application as we assume that every ice parcel is passively advected with the velocity field without any additional advection terms. For further details regarding OceanParcels please refer to Lange and van Sebille (2017). For OceanParcels to work we need to provide three dimensional velocity data covering the time frame we are interested in (i.e., the last 160 ka as this is the age of the oldest isochrone we take into account)

https://doi.org/10.5194/tc-2020-349
Preprint. Discussion started: 2 December 2020

as well as the ice-sheet's geometry (thickness and bedrock elevation) at sufficiently high temporal resolution. Naturally, the finer the temporal resolution of the ice-sheet time slice data, the more accurate the particle tracks will be. However, to prevent input data for OceanParcels from getting too large for standard python libraries (numpy, scipy, netCDF4) and memory we opted for a temporal resolution of 1 ka and 10 ka which proved to be accurate enough for the (for the most part) relatively slow ice flow in East Antarctica. We set the advection time step (Δt) to one year and for each experiment we employ $200,000$ individual tracers which we seed at the ice surface at the time of the age of the isochrone we want to compute (e.g. at 38 ka BP for the 38 ka isochrone). Misfits of the ice-sheet model state in terms of elevation and velocity field relative to the true (unknown) ice sheet state at that point in time in the past, will lead to deviations of the modeled isochrone as observed in the ice sheet today. This information can then be used to identify such misfits and improve the model representation of the ice sheet. We find that for less than 10^5 tracers, gaps in coverage due to the dispersive nature of ice flow are too large to resolve the internal layers away from ice divides. The seeding mask (i.e., the region where tracers are initiated) consists of the area with an ice thickness of more than 2200 m and surface flow slower than 7 m/a (see Figure 2 and the supplementary video). The seeding mask covers an area which entails every individual radar transect analysed here. We also tested other seeding strategies employing the IMBIE drainage basins (Zwally et al., 2012), ice divides or around ice core locations. The tracer experiments where all carried out on a laptop computer (Powerbook (2015), 2.7 GHz, 8 GB memory, OS-X: 10.13.6), with computation times between a few hours (38 ka isochrone) and 10-15 hours (160 ka isochrone), i.e., $\approx$ 1h/10ka elapsed model time.

OceanParcels provides netCDF-files consisting of the individual tracer positions in space and time. Accordingly, to extract isochrones we selected the last tracer positions and gridded them to a regular 1 km x 1 km grid (bi-linear interpolation). This provided an elevation map of the respective tracer swarm for all regions covered by the seeding mask (see Figure 3 A and supplementary video). From this elevation map we then extracted the computed tracer-, bedrock- and surface-elevation as well as the melting at the base of the ice and the corresponding geothermal heat flux (which was provided as input data) along the individual radar transects.

3 Modelled Antarctic isochrone elevations

Our main goal is the identification of systematic mismatches between predicted and observed isochrone geometry. To achieve this, we focus on three major sources of model-observation mismatches: (i) climate forcing, (ii) model parameterisation, (iii) bedrock and geothermal heat flux. As computed isochrone elevations will be affected by a superposition of uncertainties from all three sources we separate our analysis into regions where we expect only one factor to dominate. To isolate the effect of (i) climate forcing we turn to areas characterised by limited ice flow (e.g. ice domes or close to ice divides) and by a good representation of the bedrock elevation in the model (difference between input data set and local high resolution radar data). Here, we will primarily focus on Dome C as the model ensemble was tuned to match the regional ice-sheet configuration. To assess the impact of model performance and ice flow parameterisation we discuss the model-fitness to compute isochrones in regions of elevated surface velocities and in subglacial basins (bedrock below sea level) as well as the effect of different parameter choices under the same boundary conditions (climate, geothermal heat flux, bedrock topography). To test (iii) we

https://doi.org/10.5194/tc-2020-349
Preprint. Discussion started: 2 December 2020

The Cryosphere Discussions
Open Access
EGU

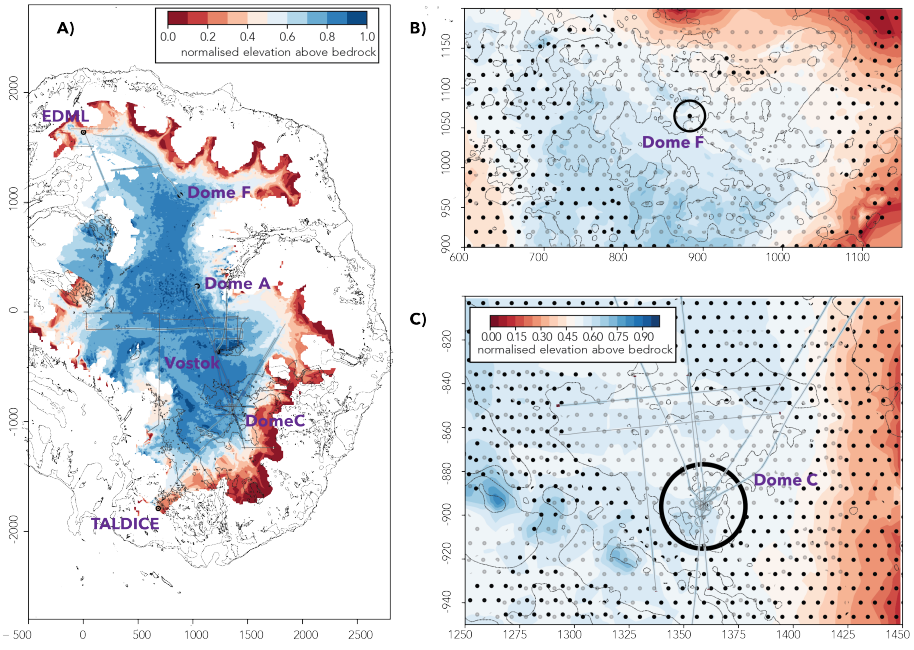

Figure 3. Computed isochrone elevation in East Antarctica. Panel A) illustrates the elevation above bedrock of the 38 ka isochrone normalised by the local ice thickness. The filled isochrone contours are overlain by radar transect observations (thin lines). Panel B) shows a blow up of the region around Dome Fuji with dotted areas where basal melt is simulated. Semi-transparent dots show results with geothermal heat flux forcing from Martos et al. (2017) and opaque dots from Shapiro and Ritzwoller (2004), respectively. Panel C) shows the area around Dome C overlain by radar observations (thin lines). Due to the small mismatch in the Dome C region only areas with strong differences between modelled and observed isochrone elevation (e.g. upper right section of C) are discernible.

analyse the impact on bedrock elevation uncertainty around Dome C and use different geothermal heat flux fields to investigate their influence on the modelled internal layer architecture.

3.1 Dome C - evaluating the paleoclimate forcing

We now turn to the first (i) of the aforementioned three main factors determining simulated isochrone elevations, the climate forcing. Due to the near cessation of surface flow at ice domes the local internal stratigraphy is by and large dominated by the regional surface mass balance history and potentially affected by basal melting due to a large ice thickness, low surface accumulation and/or elevated geothermal heat flux. Consequently, in the particular geographic setting of an ice divide, we do not expect that parameterisations of ice dynamics will have a large effect on the internal layer architecture. Therefore, we assume that model-mismatches with respect to observed isochrones are mostly due to the applied surface mass balance forcing and geothermal heat flux. To evaluate the validity of the forcing approach in Sutter et al. (2019) we turn to several radar transects in the vicinity of the DC ice core ($75°1'$ S, $123°4'$ E, see Figure 4) which satisfy the condition of low ice surface

https://doi.org/10.5194/tc-2020-349
Preprint. Discussion started: 2 December 2020

The Cryosphere
Discussions
Open Access
EGU

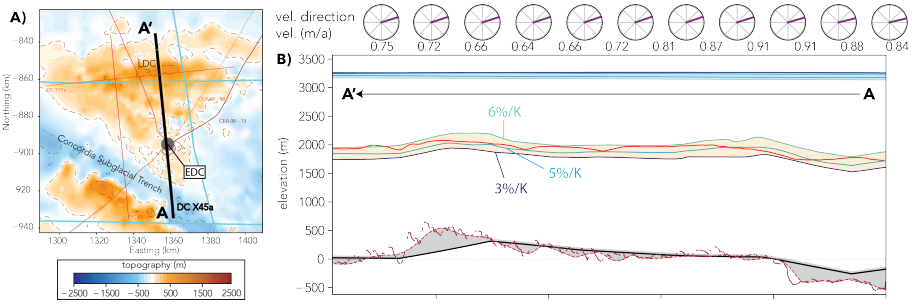

Figure 4. Transect DC-X45a with the 96 ka isochrone. Panel A) illustrates the bedrock elevation and radar transects analysed in this study crossing Dome. In B) the computed isochrone elevations for simulations with 3%, 5% and 6% precipitation change per Kelvin surface temperature change are plotted against the observed isochrone (red dashed line). Bedrock topography used in the model runs is plotted in black and bedrock elevation derived from the radar transect in brown-dashed. The gridded 1km BedMachine bedrock elevation (Morlighem et al., 2020) is plotted for comparison as well (smooth dashed purple line). The circles denote the relative flow direction and speed with respect to the radar transect.

velocities. The radar transects are discussed in Cavitte et al. (2016) and cut across an area loosely bound by Concordia Trench and Little Dome C (LDC).

In a first step we investigate which surface mass balance history during the last glacial-interglacial cycle matches best with the 96 ka isochrone along transect DC-57a, which spans from the northern end of the Concordia Subglacial Trench southward via EDC to LDC (thick black line in Figure 4 A). Isochrones are computed from the output of experiment B1-P1 in Sutter et al. (2019) using different scaling constants between temperature and accumulation anomalies ($\%K^{-1}$, 3, 5, 6, 8, i.e. percent change of accumulation for every degree of surface air temperature change) inspired by the approximate range indicated by paleo proxies (Frieler et al., 2015). Figure 4 B depicts the observed 96 ka isochrone in comparison to the simulated isochrones. The latter fit the observations reasonably well to within $\approx 2-5\%$ of the local ice thickness. According to our simulations a precipitation scaling between 5 and 6 $\%K^{-1}$ completely reproduces the 96 ka isochrone which is in accordance with ice core reconstructions from EPICA Dome C (Frieler et al., 2015). This gives us confidence that the paleo mass balance forcing approach in Sutter et al. (2019) is valid at least for the interior of the East Antarctic Ice Sheet. It is important to note, that the simulations are tuned to the geothermal heat flux data from Shapiro and Ritzwoller (2004). Comparison to simulations employing other data sets shows that the modelled isochrones fit well for GHF from Purucker (2013); An et al. (2015) but fail to reproduce the approximate isotope elevation for the high GHF from Martos et al. (2017) which produces widespread basal melting beyond (1 mm/a) in the region (see Fig. 3 C). Geothermal heat flux is uncertain for most parts of the Antarctic Ice Sheet and regional differences between published datasets can be substantial (Burton-Johnson et al., 2020; Talalay et al., 2020). Local basal melting occurs under forcing with the Shapiro data set as well but is largely limited to (0-1 mm/a) and lies between 0.25-0.5 mm/a around EDC. The computed basal melt rates with GHF from Shapiro and Ritzwoller (2004) and a temperature precipitation scaling of $6\%K^{-1}$ are similar to the ones in Passalacqua et al. (2017) which are empirically determined to fit the EPICA Dome C ice core age scale.

https://doi.org/10.5194/tc-2020-349
Preprint. Discussion started: 2 December 2020

The Cryosphere Discussions
Open Access
EGU

Above, we identified which paleo temperature-precipitation scaling leads to the best fit of modelled and observed isochrone elevations. Making use of this paleo-accumulation estimate we can plot the transient accumulation history at EDC during the last glacial interglacial cycle as well as the regional precipitation forcing during the LGM and the LIG. Figure 5 A) depicts the EDC accumulation history depending on the temperature-precipitation scaling-factor. The Holocene surface mass balance fluctuates close to the present day model estimate from the regional climate model RACMO van Wessem et al. (2014) which is used here as the present day reference climate state (ca. 3 cm/a ice equivalent) and drops to ca. 1.7 cm/a during the LGM. The observed modern surface mass balance at EDC is ≈ 2.5 cm/a (Stenni et al., 2016) i.e. our present day surface mass balance forcing is ca. 20% too high in this region. When we compare our simplified forcing with reconstructed paleo-accumulation patterns at Dome C by Cavitte et al. (2018) our estimates of paleo-accumulation differs by about $+10 - 30\%$. This is mostly due to the aforementioned overestimation in the 1979-2011 present day reference surface mass balance at EDC derived from RACMO (van Wessem et al., 2014). It is important to note, that our approach does not strive to achieve a detailed reconstruction of paleo-accumulation as done in Cavitte et al. (2018). They are fitting englacial layer horizons via a 1-D pseudo-steady ice flow model (Parrenin et al., 2017) leading to more accurate estimates of the local surface mass balance along the ice divide, while we are merely trying to establish the validity of our paleoclimate forcing approach. Nevertheless, Figure 5 illustrates that our paleo-accumulation forcing provides a surface mass balance pattern along ice divides which matches more detailed reconstructions as carried out by Cavitte et al. (2018) reasonably well.

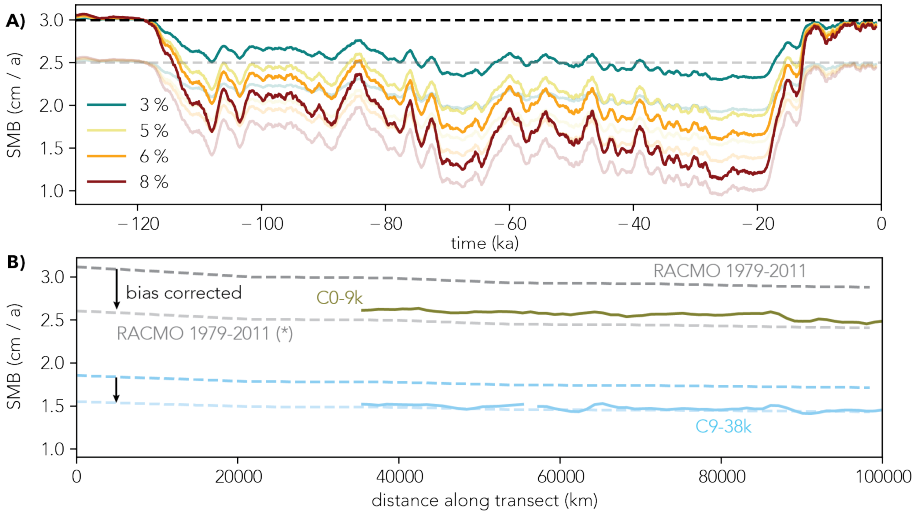

Figure 5. A) Prescribed precipitation (cm/a) over time at the EPICA Dome C ice core drill site for different temperature-precipitation scaling ($3, 5, 6, 8\%K^{-1}$). B) Green and light blue lines depict the mean 0-9 ka and 9-38 ka accumulation along transect X45a from Cavitte et al. (2018) or in (dashed) the simulated accumulation with precipitation forcing for a $7\%K^{-1}$ temperature-precipitation scaling, respectively. The semi-transparent dashed lines depict the precipitation after bias correction of the present day reference data from van Wessem et al. (2014).

https://doi.org/10.5194/tc-2020-349
Preprint. Discussion started: 2 December 2020


The Cryosphere Discussions
Open Access
EGU

The modelled isochrone elevations discussed above where computed on the basis of transient snapshots of local velocity and topography fields and show a good match to observed isochrone elevations. In the following we analyse the modelled 96 ka isochrone-elevation along transect DC-X57a for three different tracer experiments in which the velocity and ice geometry is taken from: 1. the full transient ISM-data from the 220 ka paleo-simulation with temperature-precipitation scaling of $5\%K^{-1}$ (case *pal*), 2. only the present day output of the latter (case *pd-pal*) and 3. the velocity and topography data from a present day climate equilibrium simulation (case *pd*) where the ice sheet is forced only by present day surface climate and ocean temperatures. In *pal* tracers are advected based on the respective temporally evolving ice sheet configuration; in *pd-pal* advection is based on the last time slice output (present day) of *pal* (constant velocity and topography); in *pd-pd* tracers are advected via the present day equilibrium velocity resulting from present day climate forcing. This will therefore elucidate the impact of the paleo-spinup and of the model parameterisation (ii) on computed isochrone elevations (Figure 6). The comparison between pal and pd-pal allows us to assess the influence of the transient past surface mass balance forcing and paleo-ice-flow reorganisation in pal while the comparison between pd-pal and pd-pd mainly illuminates the effect of the parameterisation of ice flow (ii) and the missing imprint of the paleo-spinup. Figure 6 shows the difference in isochronal elevation between *pal* and *pd-pal*. It is relatively small in comparison to the difference between *pal* and *pd-pd* despite the fact that surface elevations for *pd-pal* and *pd-pd* are very similar. This illustrates that tuning an ISM to present day observations and mass balance trends (*pd-pd*) might yield a suitable fit to ice-sheet surface observations but fails to capture the integrated internal layering which is a product of the paleo surface-mass-balance as well as of paleo ice-dynamics. This might have important repercussions for paleo ice-sheet studies as well as for projections of the future sea-level contribution of the Antarctic Ice Sheet, as the ice-sheet's initial state can affect its future behaviour over centennial or even decadal time scales (Seroussi et al., 2019) due to misrepresentations e.g. in the parameterisation of basal friction, the internal flow fields (and thus mass transport) and the thermal state as a consequence of overfitting. Ideally, to assess the impact of isochrone elevation calibration on ice sheet model projections, one would compare three cases where the model parameters are tuned a) via thickness/surface velocity inversion, b) against present day surface observables and paleo-proxies (ideally including a paleo spinup) and c) isochrone elevation calibration combined with b). This is work in progress and beyond the scope of this manuscript.

3.2 Caveats to modelling isochrones with large scale ice-sheet models

Differences between modelled isochrones (based on paleo-velocity fields) and their observed elevation above bedrock are small for all isochrones sampled in this study which are younger than the LIG (< 120 ka, root mean square deviation of RMSD $< 5\%$). It is striking however, that for isochrones older than 130 ka the gap between model results and observation widens (see Figure 7). Due to the lack of climate model data for glacials and interglacials preceding the LIG, we estimated the climate forcing before 130 ka BP to be a linear combination between the climate state of the LGM and the LIG using the EPICA Dome C deuterium record as an index to interpolate between the two climate states (see section 2.1 in Sutter et al. (2019)). Naturally, this approach is just an approximation of the actual transient climate conditions and therefore will necessarily lead to discrepancies in the surface mass balance as well as the ocean forcing. Another potential cause of the relatively poor representation of isochrones before 130 ka BP is the high circum-antarctic subsurface ocean temperature peak assumed for

https://doi.org/10.5194/tc-2020-349
Preprint. Discussion started: 2 December 2020

The Cryosphere
Discussions
Open Access
EGU

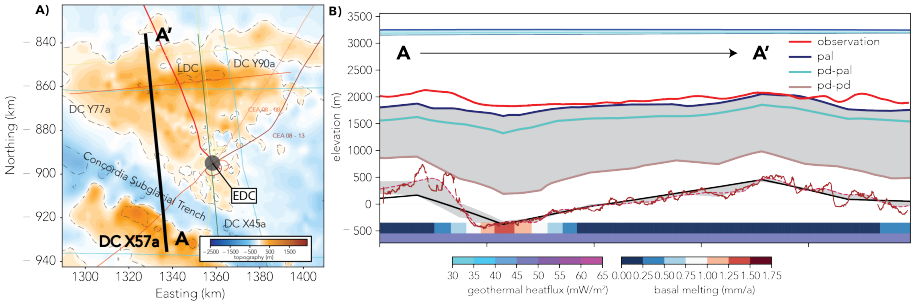

Figure 6. Comparison of the observed 96 ka X57a isochrone (red line in right panel) in the Dome C region with the model simulation: A) depicts the study area and the radar transect corresponding to the simulated and observed transect. B) paleoclimate simulation with $5\%K^{-1}$ precipitation scaling (dark blue line), present day output of the paleoclimate simulation (cyan line) and present day equilibrium simulation (brown line). The coloured bars on the bottom of B) depict the geothermal heat flux and the computed basal melt rate along the transect.

the LIG (ca. 2°C). Due to coastal thinning and potentially grounding line retreat caused by aforementioned elevated ocean temperatures this might lead to an exaggerated ice flow in the major drainage basins such as the Wilkes Basin (see Fig 9) or the Aurora Basin, in turn potentially affecting even remote regions such as Dome C. In fact, the model-data-observations mismatch is especially poor for the sections of the Dome C transects close to the Aurora Subglacial Basin which could also point to an issue with the parameterisation of basal drag in subglacial basins (see section 4). Finally, the simulations analysed in the previous sections where initialised at 220 ka BP. Therefore the model spinup for the calculations of the 130 and 160 ka isochrone elevations was only 60 and 90 ka, respectively. This could be another aspect influencing the particularly poor match between modelled and observed isochrone elevations for these ages.

Next to the uncertainties associated with paleoclimate forcing fields and ice-sheet model parameterisations the uncertainties in the basal boundary conditions (iii) applied in a large-scale paleo-ice-sheet model further complicate the computation of isochrone elevations. Uncertainties in the bedrock elevation in areas with only sparse radar observations can feature differences of several hundred meters if compared to newly acquired high-resolution radar data (Karlsson et al., 2018; Morlighem et al., 2020). This can affect the basal flow regime and corresponding thermal state of the local ice column significantly. We would expect, that line transects characterised by a bedrock profile in relatively good agreement with reality should yield a good agreement between modelled and observed isochrones as well. While this is true e.g. for some parts of transect DC-X57 in the Dome C region (see Figure 8), the assumption cannot be generalised to all East Antarctic transects discussed in this work as uncertainties in the parameterisations of ice flow, paleoclimate forcing and geothermal heat flux can have a dominating or confounding effect over differences in the observed and modelled bedrock relief. Additionally, the impact of bedrock undulations on isochrone elevation will be stronger close to bedrock and might not be observable in relatively young isochrones where the surface mass balance is the dominating factor. A further caveat is the largely unknown distribution of geothermal heat at the base of the ice which is only inferred indirectly and exhibits large differences in between data-sets Shapiro and Ritzwoller (2004); Purucker (2013); An et al. (2015); Martos et al. (2017). A complete assessment of the relative influence of basal and

https://doi.org/10.5194/tc-2020-349
Preprint. Discussion started: 2 December 2020

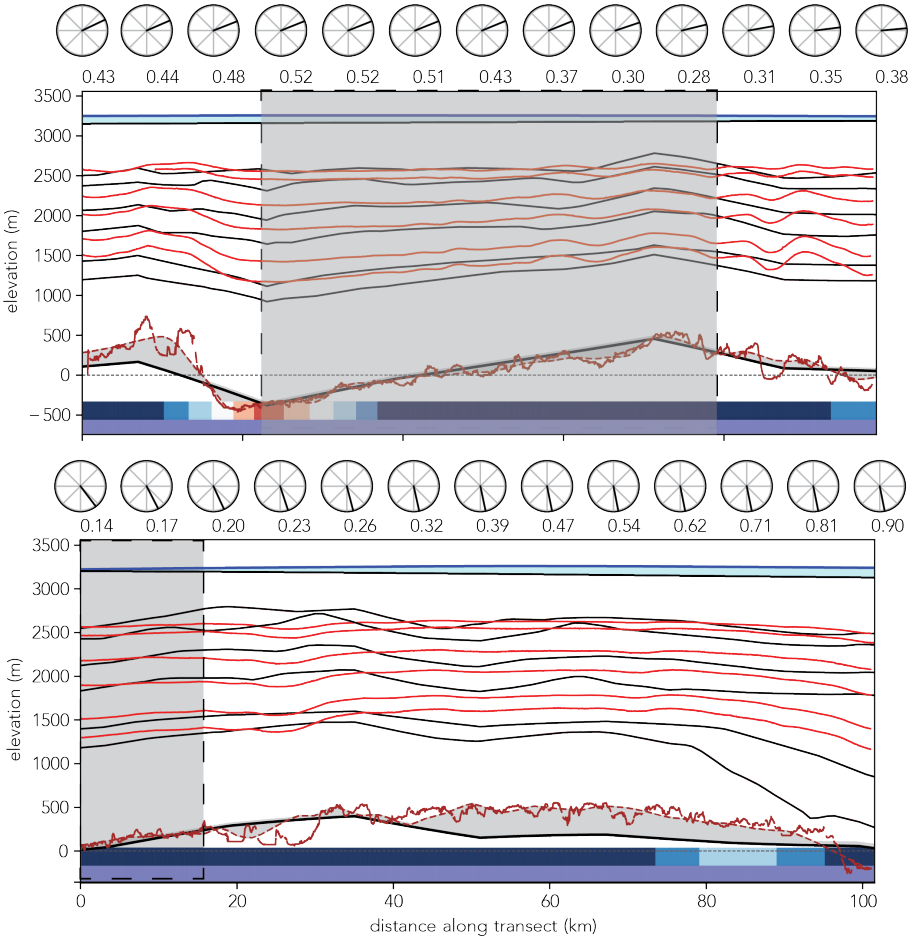

Figure 7. Modelled (black lines) and observed isochrones (red lines 38, 48, 74, 96, 130, 160 ka from top to bottom) for transect DC-X57 (upper panel) and DC-Y77 (lower panel). The grey vertical bars highlight areas with low elevation differences in the low resolution model bedrock input (black line) compared to the high resolution radar observations (red dashed lines) which generally correspond to a good match of modelled and observed isochrones. The difference between the model bedrock and the 1 km BedMachine data (Morlighem et al., 2020) is highlighted by the grey shading. The labeled circles denote the surface flow and magnitude in m/a relative to the direction of the transect. The coloured bars on the bottom of depict the geothermal heat flux and the computed basal melt rate along the transect as in Figure 6.

surface boundary conditions as well as model parameterisations on East Antarctic isochrone elevations across the whole ice column is beyond the scope of this study but could be the focus of an upcoming paleo-ice-sheet model intercomparison.

4 Large scale modelling of the internal architecture of the East Antarctic Ice Sheet

In the following, we expand our view to the whole of the East Antarctic Ice Sheet, assessing how valid the choices of model parameters and the paleo-accumulation forcing, derived from Dome C really are when it comes to simulating the evolution

https://doi.org/10.5194/tc-2020-349
Preprint. Discussion started: 2 December 2020

The Cryosphere Discussions
Open Access
EGU

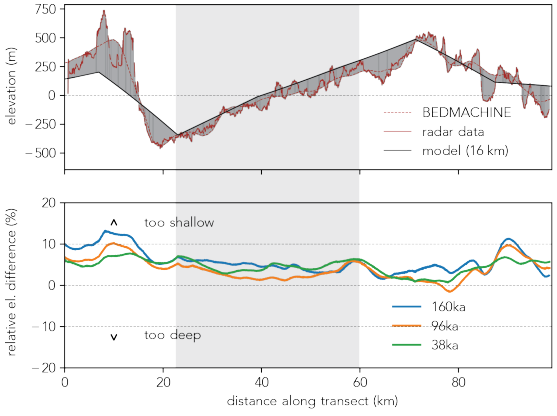

Figure 8. Illustration of bedrock uncertainty vs. relative difference between modelled and observed 38, 97 and 160 ka isochrone (DC-X57). Upper panel depicts the bedrock elevation from the model simulation based on the Bedmap2 (Fretwell et al., 2013) at 16 km resolution (black line), bedrock radar reflection (Cavitte et al., 2016) (red line) and Bedmachine Antarctica (Morlighem et al., 2020) data at 1 km resolution (red dashed line). Lower panel depicts isochrone mismatch (normalised with local ice thickness) between modelled and observed isochrone elevation.

of the whole ice-sheet. The focus on the EDC ice core region in the previous section allowed us to appreciate the impact of uncertain forcing fields and bedrock elevation on a relatively small length scale (100 km). We now turn to larger distances, where the Dome C-derived transient paleoclimate forcing and model optimisation might lead to more pronounced diversions between the modelled isochrone elevations and the radar data. We first assess the 90 ka isochrone along transect CEA-10 (see Figure 9). It starts close to TALDICE crossing the upper reaches of the Wilkes Subglacial Basin after which it traverses the Concordia Subglacial Trench, passing EDC and LDC and finally arching upwards to end at Lake Vostok (total distance ca. 1500 km).

Figure 9 illustrates nicely, that there are two main regimes covered by profile CEA-10. The northern half of the transect bottom part in Figure 9) is dominated by the imprint of the Wilkes Subglacial Basin with a large misfit between the modelled and observed isochrone. The striking excursions of the modelled isochrone elevation in Figure 9 point towards a too fast internal vertical ice motion. This could possibly be due to the heuristics involved in determining the yield stress in subglacial basins. While a spatially varying temperature-precipitation relationship could also affect the isochrone elevation in this region, this seems not to be the case here. We show this by computing the 90-ka isochrone elevation in a paleo-simulation with a temperature-precipitation relationship of $8\%\mathrm{K}^{-1}$ which cannot mitigate the drop in elevation in the first 300 km of the transect (see Figure 9). We did not test temperature precipitation relationships higher than $8\%\mathrm{K}^{-1}$, as they would be beyond what is reconstructed from East Antarctic ice cores. Geothermal heat flux can also be ruled out from being the culprit, as for the most part the thermal regime in the data set from Shapiro and Ritzwoller (2004) at Dome C is similar or even lower (of course the actual Geothermal heat flux could be much higher affecting local isochrone elevations, this could be tested in a more

https://doi.org/10.5194/tc-2020-349
Preprint. Discussion started: 2 December 2020

expansive analysis running the model with a variety of regional geothermal heat flux offsets). On the basis of the boundary conditions used here, we suggest, that the main reason for the isochrone mismatch lies in the parameterisation of basal drag and ice flow. The basal friction in the model is a function of bedrock elevation and decreases with depth, therefore it is lower in bedrock depressions especially below sea level where sliding is thus higher. Also, the relatively coarse resolution (16 km) used here leads to a "smoothed-out" bedrock profile (see Figure 8) potentially favouring faster basal ice flow. A "rougher" bedrock profile might impede sliding in drainage regions. Another aspect could be the choice of the so called "enhancement factor" in the shallow ice approximation SIA_e which is a crude tuning parameter to accommodate for anisotropic ice. Here, $SIA_e = 1.0$ which is low compared to values used in other studies (generally, a lower value of SIA_e leads to slower ice flow) so we do not expect that the enhancement factor plays a dominant role.

We now focus on the 74 ka isochrone connecting Dome Fuji ($77°32'$S, $38°70'$E) and the EDML ice core ($75°0'$S, $0°068'$E). Figure 10 illustrates the topographic characteristics of the area enclosing Dome Fuji and EDML. In contrast to Dome C which is surrounded by bedrock below sea level in the outskirts of the Aurora Subglacial Basin, the ice bed at and around Dome Fuji is elevated above sea level for several hundreds of kilometres in every direction. This means that the yield stress computed by the ISM will be very high in a large area, making the impact of sliding on internal ice velocities negligible. Both transects DML-VIII23 and DML-IV24 are characterised by mountainous subglacial terrain above sea level. Any mismatches between the observed and modelled isorchrone elevations is most probably due to uncertainties in the climate forcing or computed basal melt patterns. Basal melting at the bed of the ice along the radar tracks is unfortunately unknown, as is the temporal paleo-accumulation pattern. A direct comparison to proxy or observational data is therefore not feasible. We limit ourselves to a qualitative discussion of the model-data mismatch trying to identify persistent patterns. Looking at DML-VIII23, the modelled isochrone elevation fits well to the observed radar data (RMSD $< 5\%$ for the whole transect) and is of similar accuracy as for the 100 km Dome C data for the same transect age (RMSD $3.5 - 5.0\%$). In contrast to the whole transect DML-VIII23, where the bedrock elevation is above sea level and relatively flat, the lower half of CEA-10 is situated above a deep bedrock depression associated with low basal friction in the model. Furthermore, past elevated ice flow episodes of the marine Wilkes Basin Ice Sheet caused by thinning of the coastal ice cover e.g. during interglacials (Sutter et al., 2020) could have mediated drawdown of isochrone elevation. The comparison between DML-VIII23 and transect CEA-10 which encompasses the outskirts of the Wilkes Subglacial Basin therefore highlights a potentially methodological deficiency in the simulated internal flow and bedrock sliding as the isochrone mismatch in transect CEA-10 cannot be remedied via a surface mass balance correction.

In case of DML-IV24 a slightly different picture emerges. For the first half of the transect, the modelled isochrone is in very good agreement to the observed elevation data (except in areas with strong deviations between the 16 km BedMap topography and the high resolution radar observation), but the second half of the transect shows large deviations in the isochrone elevation leading to an overall RMSD of ca. 10% for the whole transect. In this case, it is not straightforward to identify the causes for the mismatch as the bedrock is above sea level along the whole transect and there is no clear correlation e.g. between elevated basal melt rates and dips in modelled isochrone elevation. One potential reason could be a relationship between temperature and precipitation anomalies in the EDML region which is fundamentally different from Dome C. This would affect the surface mass balance forcing and therefore the elevation of the isochrone. However, the proxy-based paleo-precipitation-

https://doi.org/10.5194/tc-2020-349
Preprint. Discussion started: 2 December 2020

The Cryosphere Discussions
Open Access
EGU

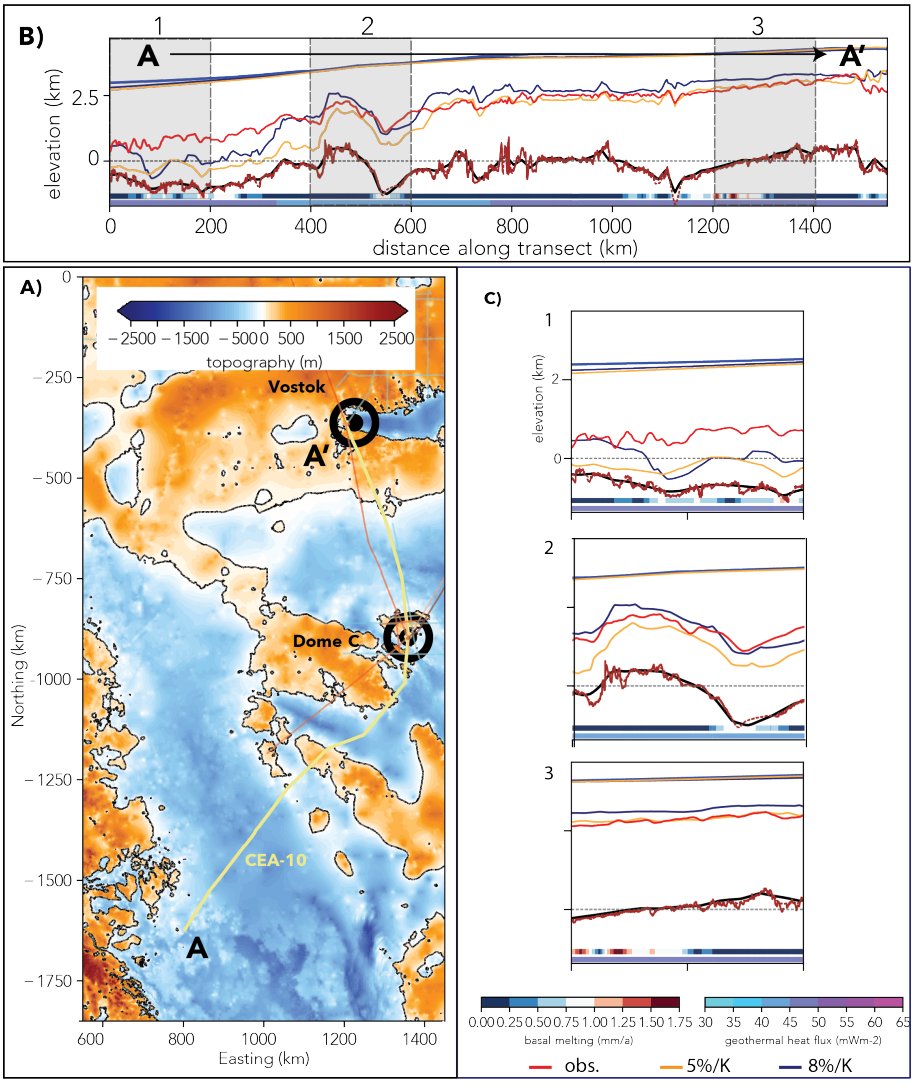

Figure 9. Overview of transect CEA-10. Panel A) shows the bedrock elevation from Morlighem et al. (2020) at 1 km resolution overlain by the CEA-10 transect in beige and other radar transects analysed in this study (thin coloured lines). Panels B) and C) illustrate the ice surface, bedrock and isochrone elevation of the 90 ka radar reflector (modelled - blue $8\%K^{-1}$, yellow $5\%K^{-1}$, observed - red) along transect CEA-10. The model bedrock elevation is depicted in black while the original radar data and the BedMachine Antarctica 1 km-grid is plotted in brown. Shaded areas in B are shown additionally in a detailed view (C). Sea level (0-elevation) is depicted by the black dotted line. The coloured bars on the bottom of B) and C) depict the geothermal heat flux and the computed basal melt rate along the transect.

https://doi.org/10.5194/tc-2020-349
Preprint. Discussion started: 2 December 2020

temperature relationship at EDML and Dome C is very similar (ca. $5.9\%\mathrm{K}^{-1}$; Frieler et al. (2015)) albeit with considerable uncertainties of $\pm 2.2\%$ and $\pm 2.8\%$ for Dome C and EDML, respectively. In fact, using the ISM results of a simulation with a precipitation-temperature relationship of $8\%\mathrm{K}^{-1}$ which is at the upper end of reconstructions for EDML, the match of the computed isochrone elevation close to EDML is improved considerably (see Figure 10). Thus, the assumption of a simple and spatially uniform accumulation/temperature scaling may be valid on the high plateau of the East Antarctic Sheet but not necessarily hold for areas close to the coast, where synoptic activity can dominate the spatial and temporal variability in precipitation (Welker et al., 2014). This could only be remedied in coupled atmosphere/ice sheet model runs that are able to resolve such synoptic activity. For computational reasons, however, this is currently not possible for such long-term runs as performed in this study. One potential solution would be to use a spatially heterogenous accumulation/temperature scaling informed by both coastal and interior ice core reconstructions.

5 Conclusions

We present the first attempt to constrain Antarctic paleoclimate forcing and parameterisations of ice flow in a continental scale ice-sheet model by comparison of simulated englacial layers against a pool of observed antarctic isochrones. We are able to reconstruct most large-scale englacial layer features and show that it is possible to identify past accumulation patterns by direct comparison of the simulated and observed internal structure of the Antarctic Ice Sheet even at coarse resolution. Furthermore, we find key isochrone elevation mismatches pointing towards poorly constrained parameterisation of basal drag especially in the proximity or above marine glaciated areas of the Antarctic Ice Sheet. The reproducibility of isochrones dramatically increases if the ice-sheet has been simulated transiently over the last several glacial-interglacial cycles. This points towards critical misrepresentations of the ice-sheets internal flow for model setups where only present day climate forcing is taken into account and the model is solely tuned against present day 2D and 1D observables. We also observe mismatches between modelled and observed isochrone elevations which can be traced back to the paleoclimate forcing employed in our model runs, which do not take into account the spatial heterogeneity of paleo temperature-precipitation relationships and effects of synoptic variability. We further show, that our paleo ice-sheet simulations suggest isochrone elevations in very good agreement with observations in slow flowing regions such as at or near ice divides. However, there seems to be a systematic overestimation of vertical advection over subglacial basins and in drainage sectors. This is most probably a commonality of all ice-sheet model setups employing similar heuristics for basal friction as we use here, i.e. the majority of ice-sheet models used for paleo-studies, raising the question whether paleo-simulations and projections of ice dynamics in subglacial basins might be subject to a systematic bias. A model intercomparison investigating isochrone elevations based on a variety of model physics and forcings could shed light on systematic misrepresentations of ice flow and, thus, internal stratigraphy in current generation ice-sheet models. Our post-processing approach would allow for such an intercomparison as it forgoes the need to implement a lagrangian tracer module into the respective ice-sheet model. We make the case, that the internal stratigraphy of the Antarctic Ice Sheet can serve as a valuable data benchmark for continental ice-sheet modelling as it provides a three dimensional tuning target which is imprinted with the complete climate and flow history of the ice-sheet. Therefore, matching

https://doi.org/10.5194/tc-2020-349
Preprint. Discussion started: 2 December 2020

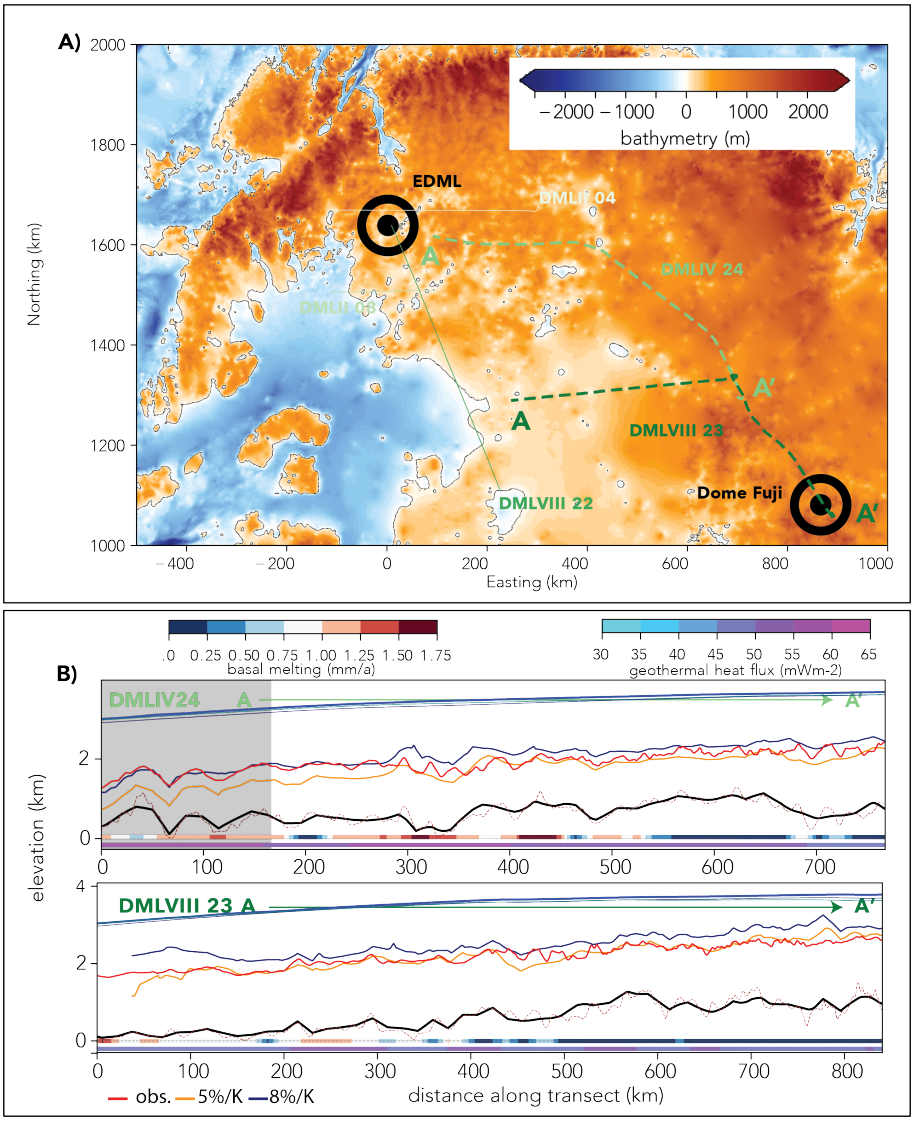

Figure 10. Overview of transect DML VIII-23 and IV-24. Panel A) shows the bedrock elevation from Morlighem et al. (2020) at 1 km resolution overlain by the DML transects in green and other radar transects analysed in this study (thin coloured lines). Panel B) illustrates the ice surface, bedrock and isochrone elevation of the 74 ka radar reflector (modelled - blue $8\%K^{-1}$, yellow $5\%K^{-1}$, observed - red). The model bedrock elevation is depicted in black while the original radar data and the BedMachine Antarctica 1 km-grid is plotted in brown. The coloured bars on the bottom of B) depict the geothermal heat flux and the computed basal melt rate along the transect.

https://doi.org/10.5194/tc-2020-349
Preprint. Discussion started: 2 December 2020

the internal structure of the ice-sheet is a powerful tool. We conclude that this approach should be used alongside traditionally employed tuning targets such as ice volume, surface velocity or grounding line positions. While analysing the match of an ISM simulation with the internal stratigraphy is not as straight forward as using surface observables, it could improve both paleo ice-sheet reconstructions as well as sea level projections due to more realistic initial ice-sheet configurations. Efforts such as AntArchitecture's to provide a compilation of all observed englacial layers will provide an invaluable data benchmark for future ice-sheet modelling efforts. Looking ahead, it would be desirable to develop a standard protocol to tune ISMs against the stratigraphy of the Antarctic Ice Sheet. This would facilitate a new generation of model simulations which are constrained by the climate and ice dynamic memory encapsulated within the ice.

Code and data availability. Both PISM and OceanParcels are open source and available via https://pism-docs.org/wiki/doku.php and http://oceanparcels.org/index.html, respectively. The isochrones from Winter et al. (2019) are available via Pangaea https://doi.pangaea.de/10.1594/PANGAEA.895528, all model data is available upon request.

Video supplement. Tracer migration from 90-0 ka BP. Tracers are seeded at the surface at 90 ka BP and transported with the ice flow over time. Coloring illustrates absolute tracer elevation. Available at https://doi.org/10.5446/50125

Author contributions. JS devised the experiments and ran the simulations. JS, HF and OE carried out the analysis. JS wrote the manuscript with contributions from HF and OE.

Competing interests. OE is CEIC of The Cryosphere

Acknowledgements. We would like to especially thank Marie Cavitte, Gwendolyn Leysinger-Vieli and Anna Winter for providing the isochrone data and helpful discussions as well as Philippe Delandmeter and Victor Onink for their support with setting up OceanParcels for the use with PISM-data. JS is grateful for funding from the Deutsche Forschungsgemeinschaft under personal grant SU 1166/1-1 (Project WANT-Ice). Hubertus Fischer gratefully acknowledges the long-term support by the Swiss National Science Foundation (SNSF). Development of PISM is supported by NSF grants PLR-1603799 and PLR-1644277 and NASA grant NNX17AG65G

https://doi.org/10.5194/tc-2020-349
Preprint. Discussion started: 2 December 2020

References

Albrecht, T., Winkelmann, R., and Levermann, A.: Glacial-cycle simulations of the Antarctic Ice Sheet with the Parallel Ice Sheet Model (PISM) - Part 2: Parameter ensemble analysis, Cryosphere, 14, 633–656, https://doi.org/10.5194/tc-14-633-2020, 2020.

An, M. J., Wiens, D. A., Zhao, Y., Feng, M., Nyblade, A., Kanao, M., Li, Y. S., Maggi, A., and Leveque, J. J.: Temperature, lithosphere-asthenosphere boundary, and heat flux beneath the Antarctic Plate inferred from seismic velocities, Journal of Geophysical Research-Solid Earth, 120, 8720–8742, https://doi.org/10.1002/2015jb011917, 2015.

Bazin, L., Landais, A., Lemieux-Dudon, B., Toyé Mahamadou Kele, H., Veres, D., Parrenin, F., Martinerie, P., Ritz, C., Capron, E., Lipenkov, V., Loutre, M.-F., Raynaud, D., Vinther, B., Svensson, A., Rasmussen, S. O., Severi, M., Blunier, T., Leuenberger, M., Fischer, H., Masson-Delmotte, V., Chappellaz, J., and Wolff, E.: An optimized multi-proxy, multi-site Antarctic ice and gas orbital chronology (AICC2012): 120-800 ka, Climate of the Past, 9, 1715–1731, https://doi.org/10.5194/cp-9-1715-2013, 2013.

Bentley, M. J., Cofaigh, C. O., Anderson, J. B., Conway, H., Davies, B., Graham, A. G. C., Hillenbrand, C. D., Hodgson, D. A., Jamieson, S. S. R., Larter, R. D., Mackintosh, A., Smith, J. A., Verleyen, E., Ackert, R. P., Bart, P. J., Berg, S., Brunstein, D., Canals, M., Colhoun, E. A., Crosta, X., Dickens, W. A., Domack, E., Dowdeswell, J. A., Dunbar, R., Ehrmann, W., Evans, J., Favier, V., Fink, D., Fogwill, C. J., Glasser, N. F., Gohl, K., Golledge, N. R., Goodwin, I., Gore, D. B., Greenwood, S. L., Hall, B. L., Hall, K., Hedding, D. W., Hein, A. S., Hocking, E. P., Jakobsson, M., Johnson, J. S., Jomelli, V., Jones, R. S., Klages, J. P., Kristoffersen, Y., Kuhn, G., Leventer, A., Licht, K., Lilly, K., Lindow, J., Livingstone, S. J., Masse, G., McGlone, M. S., McKay, R. M., Melles, M., Miura, H., Mulvaney, R., Nel, W., Nitsche, F. O., O'Brien, P. E., Post, A. L., Roberts, S. J., Saunders, K. M., Selkirk, P. M., Simms, A. R., Spiegel, C., Stolldorf, T. D., Sugden, D. E., van der Putten, N., van Ommen, T., Verfaillie, D., Vyverman, W., Wagner, B., White, D. A., Witus, A. E., Zwartz, D., and Consortium, R.: A community-based geological reconstruction of Antarctic Ice Sheet deglaciation since the Last Glacial Maximum, Quaternary Science Reviews, 100, 1–9, https://doi.org/10.1016/j.quascirev.2014.06.025, 2014.

Bingham, R., e. a.: Report of AntArchitecture Workshop, July 2017, https://www.scar.org/library/science-4/geosciences/antarchitecture/5240-antarchitecture-workshop-2017/, 2020.

Born, A.: Tracer transport in an isochronal ice-sheet model, Journal of Glaciology, 63, 22–38, https://doi.org/10.1017/jog.2016.111, 2017.

Bueler, E. and Brown, J.: Shallow shelf approximation as a "sliding law" in a thermodynamically coupled ice sheet model, J. Geophys. Res., 114, https://doi.org/10.1029/2008JF001179, http://www.agu.org/pubs/crossref/2009/2008JF001179.shtml, 2009.

Burton-Johnson, A., Dziadek, R., and Martin, C.: Review article: Geothermal heat flow in Antarctica: current and future directions, The Cryosphere, 14, 3843–3873, https://doi.org/10.5194/tc-14-3843-2020, 2020.

Cavitte, M. G. P., Blankenship, D. D., Young, D. A., Schroeder, D. M., Parrenin, F., Lemeur, E., Macgregor, J. A., and Siegert, M. J.: Deep radiostratigraphy of the East Antarctic plateau: connecting the Dome C and Vostok ice core sites, Journal of Glaciology, 62, 323–334, https://doi.org/10.1017/jog.2016.11, 2016.

Cavitte, M. G. P., Parrenin, F., Ritz, C., Young, D. A., Van Liefferinge, B., Blankenship, D. D., Frezzotti, M., and Roberts, J. L.: Accumulation patterns around Dome C, East Antarctica, in the last 73 kyr, Cryosphere, 12, 1401–1414, https://doi.org/10.5194/tc-12-1401-2018, 2018.

Clarke, G. K. C., Marshall, S. J., Rybak, O., and Huybrechts, P.: A comparison of Eulerian and Lagrangian methods for dating in numerical ice-sheet models, Annals of Glaciology, Vol 37, 37, 150–158, ann Glaciol, 2003.

Clarke, G. K. C., Lhomme, N., and Marshall, S. J.: Tracer transport in the Greenland ice sheet: three-dimensional isotopic stratigraphy, Quaternary Science Reviews, 24, 155–171, https://doi.org/10.1016/J.Quascirev.2004.08.021, quaternary Sci Rev, 2005.

DeConto, R. M. and Pollard, D.: Contribution of Antarctica to past and future sea-level rise, Nature, 531, 591–597, https://doi.org/10.1038/nature17145, 2016.

Delandmeter, P. and van Sebille, E.: The Parcels v2.0 Lagrangian framework: new field interpolation schemes, Geoscientific Model Development, 12, 3571–3584, https://doi.org/10.5194/gmd-12-3571-2019, 2019.

Dutton, A., Carlson, A. E., Long, A. J., Milne, G. A., Clark, P. U., DeConto, R., Horton, B. P., Rahmstorf, S., and Raymo, M. E.: Sea-level rise due to polar ice-sheet mass loss during past warm periods, Science, 349, https://doi.org/10.1126/science.aaa4019, 2015.

Edwards, T. L., Brandon, M. A., Durand, G., Edwards, N. R., Golledge, N. R., Holden, P. B., Nias, I. J., Payne, A. J., Ritz, C., and Wernecke, A.: Revisiting Antarctic ice loss due to marine ice-cliff instability, Nature, 566, 58–+, https://doi.org/10.1038/s41586-019-0901-4, 2019.

Eisen, O., Wilhelms, F., Steinhage, D., and Schwander, J.: Improved method to determine RES-reflector depths from ice-core profiles of permittivity and conductivity, Journal of Glaciology, 52, 299–310, https://doi.org/10.3189/172756506781828674, 2006.

Feldmann, J., Albrecht, T., Khroulev, C., Pattyn, F., and Levermann, A.: Resolution-dependent performance of grounding line motion in a shallow model compared with a full-Stokes model according to the MISMIP3d intercomparison, Journal of Glaciology, 60, 353–360, https://doi.org/10.3189/2014JoG13J093, 2014.

Fretwell, P., Pritchard, H. D., Vaughan, D. G., Bamber, J. L., Barrand, N. E., Bell, R., Bianchi, C., Bingham, R. G., Blankenship, D. D., Casassa, G., Catania, G., Callens, D., Conway, H., Cook, A. J., Corr, H. F. J., Damaske, D., Damm, V., Ferraccioli, F., Forsberg, R., Fujita, S., Gim, Y., Gogineni, P., Griggs, J. A., Hindmarsh, R. C. A., Holmlund, P., Holt, J. W., Jacobel, R. W., Jenkins, A., Jokat, W., Jordan, T., King, E. C., Kohler, J., Krabill, W., Riger-Kusk, M., Langley, K. A., Leitchenkov, G., Leuschen, C., Luyendyk, B. P., Matsuoka, K., Mouginot, J., Nitsche, F. O., Nogi, Y., Nost, O. A., Popov, S. V., Rignot, E., Rippin, D. M., Rivera, A., Roberts, J., Ross, N., Siegert, M. J., Smith, A. M., Steinhage, D., Studinger, M., Sun, B., Tinto, B. K., Welch, B. C., Wilson, D., Young, D. A., Xiangbin, C., and Zirizzotti, A.: Bedmap2: improved ice bed, surface and thickness datasets for Antarctica, Cryosphere, 7, 375–393, https://doi.org/10.5194/Tc-7-375-2013, 2013.

Frieler, K., Clark, P. U., He, F., Buizert, C., Reese, R., Ligtenberg, S. R. M., van den Broeke, M. R., Winkelmann, R., and Levermann, A.: Consistent evidence of increasing Antarctic accumulation with warming, Nature Climate Change, 5, 348–352, 2015.

Garbe, J., Albrecht, T., Levermann, A., Donges, J. F., and Winkelmann, R.: The hysteresis of the Antarctic Ice Sheet, Nature, 585, 538–544, https://doi.org/10.1038/s41586-020-2727-5, 2020.

Gladstone, R. M., Payne, A. J., and Cornford, S. L.: Parameterising the grounding line in flow-line ice sheet models, Cryosphere, 4, 605–619, https://doi.org/10.5194/Tc-4-605-2010, 2010.

Goelles, T., Grosfeld, K., and Lohmann, G.: Semi-Lagrangian transport of oxygen isotopes in polythermal ice sheets: implementation and first results, Geoscientific Model Development, 7, 1395–1408, https://doi.org/10.5194/gmd-7-1395-2014, geosci Model Dev, 2014.

Goelzer, H., Nowicki, S., Payne, A., Larour, E., Seroussi, H., Lipscomb, W. H., Gregory, J., Abe-Ouchi, A., Shepherd, A., Simon, E., Agosta, C., Alexander, P., Aschwanden, A., Barthel, A., Calov, R., Chambers, C., Choi, Y., Cuzzone, J., Dumas, C., Edwards, T., Felikson, D., Fettweis, X., Golledge, N. R., Greve, R., Humbert, A., Huybrechts, P., Le clec'h, S., Lee, V., Leguy, G., Little, C., Lowry, D. P., Morlighem, M., Nias, I., Quiquet, A., Rückamp, M., Schlegel, N.-J., Slater, D., Smith, R., Straneo, F., Tarasov, L., van de Wal, R., and van den Broeke, M.: The future sea-level contribution of the Greenland ice sheet: a multi-model ensemble study of ISMIP6, The Cryosphere Discussions, 2020, 1–43, https://doi.org/10.5194/tc-2019-319, 2020.

Hindmarsh, R. C. A., Vieli, G. J. M. C. L., and Parrenin, F.: A large-scale numerical model for computing isochrone geometry, Annals of Glaciology, 50, 130–140, https://doi.org/10.3189/172756409789097450, 2009.

Huybrechts, P., Rybak, O., Pattyn, F., Ruth, U., and Steinhage, D.: Ice thinning, upstream advection, and non-climatic biases for the upper 89% of the EDML ice core from a nested model of the Antarctic ice sheet, Climate of the Past, 3, 577–589, https://doi.org/10.5194/cp-3-577-2007, clim Past, 2007.

Joughin, I., Smith, B., Howat, I., and Scambos, T.: MEaSUREs Greenland Ice Sheet Velocity Map from InSAR Data, Version 2., Boulder, Colorado USA. NASA National Snow and Ice Data Center Distributed Active Archive Center, https://doi.org/10.5067/OC7B04ZM9G6Q, 2015, updated 2018.

Jouvet, G., Röllin, S., Sahli, H., Corcho, J., Gnägi, L., Compagno, L., Sidler, D., Schwikowski, M., Bauder, A., and Funk, M.: Dating the ice of Gauligletscher, Switzerland, based on surface radionuclide contamination and ice flow modeling, The Cryosphere Discussions, 2020, 1–28, https://doi.org/10.5194/tc-2020-142, 2020.

Jouzel, J., Masson-Delmotte, V., Cattani, O., Dreyfus, G., Falourd, S., Hoffmann, G., Minster, B., Nouet, J., Barnola, J. M., Chappellaz, J., Fischer, H., Gallet, J. C., Johnsen, S., Leuenberger, M., Loulergue, L., Luethi, D., Oerter, H., Parrenin, F., Raisbeck, G., Raynaud, D., Schilt, A., Schwander, J., Selmo, E., Souchez, R., Spahni, R., Stauffer, B., Steffensen, J. P., Stenni, B., Stocker, T. F., Tison, J. L., Werner, M., and Wolff, E. W.: Orbital and millennial Antarctic climate variability over the past 800,000 years, Science, 317, 793–796, https://doi.org/10.1126/Science.1141038, 2007.

Karlsson, N. B., Binder, T., Eagles, G., Helm, V., Pattyn, F., Van Liefferinge, B., and Eisen, O.: Glaciological characteristics in the Dome Fuji region and new assessment for "Oldest Ice", Cryosphere, 12, 2413–2424, https://doi.org/10.5194/tc-12-2413-2018, 2018.

Konrad, H., Bohleber, P., Wagenbach, D., Vincent, C., and Eisen, O.: Determining the age distribution of Colle Gnifetti, Monte Rosa, Swiss Alps, by combining ice cores, ground-penetrating radar and a simple flow model, Journal of Glaciology, 59, 179?189, https://doi.org/10.3189/2013JoG12J072, 2013.

Lange, M. and van Sebille, E.: Parcels v0.9: prototyping a Lagrangian ocean analysis framework for the petascale age, Geoscientific Model Development, 10, 4175–4186, https://doi.org/10.5194/gmd-10-4175-2017, 2017.

Leysinger-Vieli, G. J. M. C. L., Hindmarsh, R. C. A., Siegert, M. J., and Bo, S.: Time-dependence of the spatial pattern of accumulation rate in East Antarctica deduced from isochronic radar layers using a 3-D numerical ice flow model, Journal of Geophysical Research-Earth Surface, 116, https://doi.org/10.1029/2010jf001785, 2011.

Lhomme, N., Clarke, G. K. C., and Marshall, S. J.: Tracer transport in the Greenland Ice Sheet: constraints on ice cores and glacial history, Quaternary Science Reviews, 24, 173–194, https://doi.org/10.1016/J.Quascirev.2004.08.020, quaternary Sci Rev, 2005a.

Lhomme, N., Clarke, G. K. C., and Ritz, C.: Global budget of water isotopes inferred from polar ice sheets, Geophysical Research Letters, 32, https://doi.org/10.1029/2005gl023774, 2005b.

Martos, Y. M., Catalan, M., Jordan, T. A., Golynsky, A., Golynsky, D., Eagles, G., and Vaughan, D. G.: Heat Flux Distribution of Antarctica Unveiled, Geophysical Research Letters, 44, 11 417–11 426, https://doi.org/10.1002/2017gl075609, 2017.

Morlighem, M., Williams, C. N., Rignot, E., An, L., Arndt, J. E., Bamber, J. L., Catania, G., Chauche, N., Dowdeswell, J. A., Dorschel, B., Fenty, I., Hogan, K., Howat, I., Hubbard, A., Jakobsson, M., Jordan, T. M., Kjeldsen, K. K., Millan, R., Mayer, L., Mouginot, J., Noel, B. P. Y., O'Cofaigh, C., Palmer, S., Rysgaard, S., Seroussi, H., Siegert, M. J., Slabon, P., Straneo, F., van den Broeke, M. R., Weinrebe, W., Wood, M., and Zinglersen, K. B.: BedMachine v3: Complete Bed Topography and Ocean Bathymetry Mapping of Greenland From Multibeam Echo Sounding Combined With Mass Conservation, Geophysical Research Letters, 44, 11 051–11 061, https://doi.org/10.1002/2017gl074954, 2017.

Morlighem, M., Rignot, E., Binder, T., Blankenship, D., Drews, R., Eagles, G., Eisen, O., Ferraccioli, F., Forsberg, R., Fretwell, P., Goel, V., Greenbaum, J. S., Gudmundsson, H., Guo, J. X., Helm, V., Hofstede, C., Howat, I., Humbert, A., Jokat, W., Karlsson, N. B., Lee, W. S.,

Matsuoka, K., Millan, R., Mouginot, J., Paden, J., Pattyn, F., Roberts, J., Rosier, S., Ruppel, A., Seroussi, H., Smith, E. C., Steinhage, D., Sun, B., van den Broeke, M. R., van Ommen, T. D., van Wessem, M., and Young, D. A.: Deep glacial troughs and stabilizing ridges unveiled beneath the margins of the Antarctic ice sheet, Nature Geoscience, 13, 132–+, https://doi.org/10.1038/s41561-019-0510-8, 2020.

Mouginot, J., Scheuchl, B., and Rignot, E.: MEaSUREs Annual Antarctic Ice Velocity Maps 2005-2017, Version 1., Boulder, Colorado USA. NASA National Snow and Ice Data Center Distributed Active Archive Center, https://doi.org/0.5067/9T4EPQXTJYW9, 2017, updated 2017.

Parrenin, F., Cavitte, M. G. P., Blankenship, D. D., Chappellaz, J., Fischer, H., Gagliardini, O., Masson-Delmotte, V., Passalacqua, O., Ritz, C., Roberts, J., Siegert, M. J., and Young, D. A.: Is there 1.5-million-year-old ice near Dome C, Antarctica?, Cryosphere, 11, 2427–2437, https://doi.org/10.5194/tc-11-2427-2017, 2017.

Passalacqua, O., Ritz, C., Parrenin, F., Urbini, S., and Frezzotti, M.: Geothermal flux and basal melt rate in the Dome C region inferred from radar reflectivity and heat modelling, Cryosphere, 11, 2231–2246, https://doi.org/10.5194/tc-11-2231-2017, 2017.

Passalacqua, O., Cavitte, M., Gagliardini, O., Gillet-Chaulet, F., Parrenin, F., Ritz, C., and Young, D.: Brief communication: Candidate sites of 1.5 Myr old ice 37 km southwest of the Dome C summit, East Antarctica, The Cryosphere, 12, 2167–2174, https://doi.org/10.5194/tc-12-2167-2018, 2018.

Pattyn, F.: The paradigm shift in Antarctic ice sheet modelling, Nature Communications, 9, https://doi.org/10.1038/s41467-018-05003-z, 2018.

Pfeiffer, M. and Lohmann, G.: Greenland Ice Sheet influence on Last Interglacial climate: global sensitivity studies performed with an atmosphere-ocean general circulation model, Climate of the Past, 12, 1313–1338, https://doi.org/10.5194/cp-12-1313-2016, 2016.

Purucker, M. E.: Geothermal heat flux data set based on low res- olution observations collected by the CHAMP satellite be- tween 2000 and 2010, and produced from the MF-6 model following the technique described in Fox Maule et al. (2005), retrieved from: https:core2.gsfc.nasa.govresearchpuruckerheatflux_updates.html, 2013.

Seroussi, H., Nowicki, S., Simon, E., Abe-Ouchi, A., Albrecht, T., Brondex, J., Cornford, S., Dumas, C., Gillet-Chaulet, F., Goelzer, H., Golledge, N. R., Gregory, J. M., Greve, R., Hoffman, M. J., Humbert, A., Huybrechts, P., Kleiner, T., Larourl, E., Leguy, G., Lipscomb, W. H., Lowry, D., Mengel, M., Morlighem, M., Pattyn, F., Payne, A. J., Pollard, D., Price, S. F., Quiquet, A., Reerink, T. J., Reese, R., Rodehacke, C. B., Schlegel, N. J., Shepherd, A., Sun, S. N., Sutter, J., Van Breedam, J., van de Wal, R. S. W., Winkelmann, R., and Zhang, T.: initMIP-Antarctica: an ice sheet model initialization experiment of ISMIP6, Cryosphere, 13, 1441–1471, https://doi.org/10.5194/tc-13-1441-2019, 2019.

Seroussi, H., Nowicki, S., Payne, A. J., Goelzer, H., Lipscomb, W. H., Abe Ouchi, A., Agosta, C., Albrecht, T., Asay-Davis, X., Barthel, A., Calov, R., Cullather, R., Dumas, C., Gladstone, R., Golledge, N., Gregory, J. M., Greve, R., Hatterman, T., Hoffman, M. J., Humbert, A., Huybrechts, P., Jourdain, N. C., Kleiner, T., Larour, E., Leguy, G. R., Lowry, D. P., Little, C. M., Morlighem, M., Pattyn, F., Pelle, T., Price, S. F., Quiquet, A., Reese, R., Schlegel, N.-J., Shepherd, A., Simon, E., Smith, R. S., Straneo, F., Sun, S., Trusel, L. D., Van Breedam, J., van de Wal, R. S. W., Winkelmann, R., Zhao, C., Zhang, T., and Zwinger, T.: ISMIP6 Antarctica: a multi-model ensemble of the Antarctic ice sheet evolution over the 21st century, The Cryosphere Discussions, 2020, 1–54, https://doi.org/10.5194/tc-2019-324, 2020.

Shapiro, N. M. and Ritzwoller, M. H.: Inferring surface heat flux distributions guided by a global seismic model: particular application to Antarctica, Earth and Planetary Science Letters, 223, 213–224, https://doi.org/10.1016/J.Epsl.2004.04.011, 2004.

Stenni, B., Scarchilli, C., Masson-Delmotte, V., Schlosser, E., Ciardini, V., Dreossi, G., Grigioni, P., Bonazza, M., Cagnati, A., Karlicek, D., Risi, C., Udisti, R., and Valt, M.: Three-year monitoring of stable isotopes of precipitation at Concordia Station, East Antarctica, Cryosphere, 10, 2415–2428, https://doi.org/10.5194/tc-10-2415-2016, 2016.

Sutter, J., Fischer, H., Grosfeld, K., Karlsson, N. B., Kleiner, T., Van Liefferinge, B., and Eisen, O.: Modelling the Antarctic Ice Sheet across the mid-Pleistocene transition - implications for Oldest Ice, Cryosphere, 13, 2023–2041, https://doi.org/10.5194/tc-13-2023-2019, 2019.

Sutter, J., Eisen, O., Werner, M., Grosfeld, K., Kleiner, T., and Fischer, H.: Limited Retreat of the Wilkes Basin Ice Sheet During the Last Interglacial, Geophysical Research Letters, 47, https://doi.org/10.1029/2020GL088131, 2020.

Talalay, P., Li, Y., Augustin, L., Clow, G. D., Hong, J., Lefebvre, E., Markov, A., Motoyama, H., and Ritz, C.: Geothermal heat flux from measured temperature profiles in deep ice boreholes in Antarctica, The Cryosphere, 14, 4021–4037, https://doi.org/10.5194/tc-14-4021-2020, https://tc.copernicus.org/articles/14/4021/2020/, 2020.

the PISM authors: PISM, a Parallel Ice Sheet Model, http://www.pism-docs.org, 2015.

van Wessem, J. M., Reijmer, C. H., Morlighem, M., Mouginot, J., Rignot, E., Medley, B., Joughin, I., Wouters, B., Depoorter, M. A., Bamber, J. L., Lenaerts, J. T. M., van de Berg, W. J., van den Broeke, M. R., and van Meijgaard, E.: Improved representation of East Antarctic surface mass balance in a regional atmospheric climate model, Journal of Glaciology, 60, 761–770, https://doi.org/10.3189/2014JoG14J051, 2014.

Veres, D., Bazin, L., Landais, A., Kele, H. T. M., Lemieux-Dudon, B., Parrenin, F., Martinerie, P., Blayo, E., Blunier, T., Capron, E., Chappellaz, J., Rasmussen, S. O., Severi, M., Svensson, A., Vinther, B., and Wolff, E. W.: The Antarctic ice core chronology (AICC2012): an optimized multi-parameter and multi-site dating approach for the last 120 thousand years, Climate of the Past, 9, 1733–1748, https://doi.org/10.5194/cp-9-1733-2013, 2013.

Welker, C., Martius, O., Froidevaux, P., Reijmer, C. H., and Fischer, H.: A climatological analysis of high-precipitation events in Dronning Maud Land, Antarctica, and associated large-scale atmospheric conditions, Journal of Geophysical Research: Atmospheres, 119, 11,932–11,954, https://doi.org/10.1002/2014JD022259, 2014.

Winkelmann, R., Martin, M. A., Haseloff, M., Albrecht, T., Bueler, E., Khroulev, C., and Levermann, A.: The Potsdam Parallel Ice Sheet Model (PISM-PIK) - Part 1: Model description, Cryosphere, 5, 715–726, https://doi.org/10.5194/Tc-5-715-2011, 2011a.

Winkelmann, R., Martin, M. A., Haseloff, M., Albrecht, T., Bueler, E., Khroulev, C., and Levermann, A.: The Potsdam Parallel Ice Sheet Model (PISM-PIK) Part 1: Model description, The Cryosphere, 5, 715–726, http://www.the-cryosphere.net/5/715/2011/tc-5-715-2011.pdf, 2011b.

Winter, A., Steinhage, D., Arnold, E. J., Blankenship, D. D., Cavitte, M. G. P., Corr, H. F. J., Paden, J. D., Urbini, S., Young, D. A., and Eisen, O.: Comparison of measurements from different radio-echo sounding systems and synchronization with the ice core at Dome C, Antarctica, The Cryosphere, 11, 653–668, https://doi.org/10.5194/tc-11-653-2017, 2017.

Winter, A., Steinhage, D., Creyts, T. T., Kleiner, T., and Eisen, O.: Age stratigraphy in the East Antarctic Ice Sheet inferred from radio-echo sounding horizons, Earth System Science Data, 11, 1069–1081, https://doi.org/10.5194/essd-11-1069-2019, 2019.

Zwally, H. J., Giovinetto, M. B., Beckley, M. A., and Saba, J. L.: Antarctic and Greenland Drainage Systems, GSFC Cryospheric Sciences Laboratory, 2012.